We are IntechOpen, the world's leading publisher of Open Access books Built by scientists, for scientists

4,800
Open access books available

122,000
International authors and editors

135M
Downloads

Our authors are among the

154
Countries delivered to

TOP 1%
most cited scientists

12.2%
Contributors from top 500 universities

WEB OF SCIENCE™

Selection of our books indexed in the Book Citation Index in Web of Science™ Core Collection (BKCI)

Interested in publishing with us?
Contact book.department@intechopen.com

Numbers displayed above are based on latest data collected.
For more information visit www.intechopen.com

Chapter 5

Towards 50% Efficiency in Solar Cells

Luis M. Hernández, Armando Contreras-Solorio, Agustín Enciso, Carlos I. Cabrera, Maykel Courel, James P. Connolly and Julio C. Rimada

Additional information is available at the end of the chapter

http://dx.doi.org/10.5772/59616

1. Introduction

High-efficiency solar cells are of interest to further decrease the cost of solar energy. Conventional solar cells are based on single junction semiconductor structures and its efficiency limit is constrained by the Shockley-Queisser limit [1] to 31%. Among the several concepts for ultra-high-efficiency photovoltaic cells, in this chapter will be presented two: quantum well solar cell and superlattice solar cells.

These approaches consist of a p-i-n solar cell of wider bandgap semiconductor (called barrier or host material) with several very thin layers of another semiconductor of lower bandgap inserted into the intrinsic region, which constitutes multiple quantum well or superlattice system. The photon absorption is then enhanced to lower energies than the bandgap of the host material, adressing one of the fundamental losses of single-junction solar cells, improving the spectral response of the solar cell in the energy region below the absorption edge of host material.

This idea was pioneered by Barnham and Duggan in 1990 [2] when they proposed the quantum well solar cell (QWSC). The superlattice solar cell (SLSC) is a more recent proposal [3], which extends the QWSC concept to the case when tunneling probability of photogenerated carriers of adjacent wells is greatly increased, and the carriers are no longer localized in individual wells. Both approaches are based on the use of nanotechnology, by the exploiting of the quantum effects of the nanostructures presented, therefore the proper understanding and calculation of the quantum effects on the solar cell operation parameters is of crucial importance.

Improving the spectral response of the cell by absorbing low energy photons from the solar spectrum is important in order to obtain extra photocurrent and therefore an increment in the short-circuit current. Nevertheless, a drop in open circuit voltage (V_{OC}) of the device has been observed, due to carrier losses caused by inclusion of lower bandgap material and the interfaces, but this voltage loss could be overcompensated by the increased short-circuit current (I_{SC}) from the quantum wells as has benn demonstrated by Nelson et al[4].

In the quantum well solar cell, as the quantum wells are inserted in the intrinsic region, the built-in electric field of the depletion layer drives to an efficient collection of carriers photo-generated in the wells. Quantum efficiency (QE) modeling showed that escape efficiency from the wells is practically unity[5], leading to an enhanced photo-current. In the case of SLSC, as the spuperlattice is obtained by tuning the quantum well width in order to maximise the tunnel probability between adjacent wells, the carriers are spreaded out through the whole superlattice via continuous minibands [6] and as a consequence obtain high conductivity and delocalisation of photogenerated carriers in the minibands decreasing the recombination. QWSC or SLSC can also be tuned, playing with material structure and compositions, in order to diminish the mistmatch between the incident spectrum and the spectral absorption properties of the device.

GaAs solar cells currently hold the world efficiency record for single-junction solar cells [7], hence the improvement of GaAs based solar cell could be important to enhance solar cell performance. The use of GaAs as host material for the design of a QWSC or SLSC would be, then, the best option. However, lattice mismatch issues place an upper limit on the quantity of quantum wells that can be contained in the intrinsic region before strain relaxation takes place, compromising the open circuit voltage. The first attempts included strained GaAs/InGaAs QWSCs, but they shown not enough quantum well absorption to increase the short-circuit current in order to overcome the loss in the Voc resulting from dislocations [8].

As a solution to the lattice mismatch problem was the insertion of strain-balanced GaAsP/InGaAs quantum wells and barriers into the intrinsic region [9]. The GaAsP/InGaAs strain-balanced quantum well solar cell (SB-QWSC) has shown an impressive performance, achieving 27% conversion efficiency at 320 suns concentration [10]. Furthermore, the SB-QWSC can offer some other advantages if used in a tandem, in the substitution of the current-limited GaAs cell in the design of high-concentration triple-junction cells which potentially could exceed the performance over the conventional metamorphic approach. These include: the absence of dislocations, dark-current dominated by radiative recombination at high incident light concentration, and so the possibility of using radiative recycling to enhance efficiency and the ability to optimize the middle cell absorption edge of the tandem for different spectral conditions.

Another novel material system proposed is the dilute nitride (GaIn)(NAs) lattice matched to GaAs. This compound is obtaining growing interest in recent years due to its very unique physical properties and a wide range of possible device applications. The band gap of GaAs decreases rapidly with the addition of small atomic fractions of nitrogen [11], besides the addition of In to GaNAs does not only provide a lattice matched material to GaAs and also decreases the band gap. A approach, using GaInNAs subcells, has been formulated to enhance the efficiency of existing triple and quadruple junction solar cells [12]. Nonetheless, so far, the poor minority carrier properties and doping issues specific to bulk dilute nitrides have frustrated the success of this approach. A different strategy has been published by Freundlich et al [13], where multiple quantum wells of GaNAs are growth inside the intrinsic region of conventional GaAs p-i-n solar cells. The authors showed a short-circuit current about 25 A/m^2 without anti-reflection coating (ARC) and open circuit voltages approximately 0.6 V, although much smaller than those reported for conventional GaAs solar cells, certainly due to high interface recombination as consequence of the lattice mismatch between GaAs and GaNAs layers.

http://dx.doi.org/10.5772/59616

In this chapter, we examine a general theoretical model for QWSC, which is applied to p-i(QW)-n QWSC of different material systems. Firstly we will apply it to an AlGaAs/GaAs QWSC, and will show that conversion efficiencies are significantly enhanced when compared with the corresponding AlGaAs baseline solar cell. Open circuit voltage, current densities, I-V curves and conversion efficiencies are calculated as function of the well and barrier band gaps, the width and depth of the wells, the number of the wells in the intrinsic region. We will take into account the light absorption by the energy levels in the quantum wells, and we show that for certain values of the studied parameters, the conversion efficiencies of the quantum well solar cell are higher than that of the corresponding homogenous p-i-n solar cell.

This theoretical model when applied to the study of AlGaAs/GaAs SLSC, also allows the determination of performance parameters (short-circuit current density, open-circuit voltage, and conversion efficiency) behavior as a function of absorption and recombination mechanisms. We present a comparative study between AlGaAs/GaAs SLSC and QWSC, which could predict the possible advantages for the use of the SLSC. A variably spaced semiconductor super-lattice was optimized to enhance the resonant tunneling between adjacent wells following the method reported by Reyes-Gómez et al. [14]. A discussion about the conditions where the SLSC performance overcomes that of QWSC is addressed. Our approach will be focused on examining the viability of the SLSC for its possible use and to clarify if they present advantages over QWSC.

Following, the model is then applied to a GaAsP/InGaAs/GaAs SB-QWSC, demostrating that high efficiency devices are feasible. Our model takes into account the influence of the strain over the energy bands of the material. The impact of tensile and compressive strain on the band structure for both conduction band and valence band are calculated in order determine the electron and hole dispersion relation $E(\mathbf{k_B})$. Similarly, the optical transitions in quantum well and barriers as a function of tensile and compressive strain are evaluated to calculate the quantum efficiency, dark current and photo-current and compared with experimental data. The broken degeneracy of the valence band due to the effect of the strain is also studied, which causes the suppression of a transition that contributes to photon emission from the edge of the quantum wells. We study both, the emission light polarized in the plane perpendicular (TM) to the quantum well which couples exclusively to the light hole transition and the emission polarized in the plane of the quantum wells (TE) which couples mainly to the heavy hole transition. It is found that the spontaneous emission rates TM and TE increase when the quantum wells are deeper. The addition of a distributed Bragg reflector can substantially increase the photocurrent while decreasing the radiative recombination current. We examine the impact of the photon recycling effect on SB-QWSC performance. Then, GaAsP/InGaAs/GaAs solar cell is optimized to reach the maximum performance by evaluating the current-voltage curves under illumination. Our model was used to determine the highest efficiencies for cells containing quantum wells under varying degrees of strain, but it could also allow the optimization of the photocurrent or the open circuit voltage in a triple-junction concentrator cell based on a SB-QWSC middle cell.

Another approach, where GaAs/GaInNAs multiple quantum wells and superlattice are added within the intrinsic region of conventional GaAs p-i-n solar cells is also presented. First, the model is applied to GaAs/GaInNAs QWSC in order to study the conversion efficiency as a function of nanostructure parameters as wells width and depth. On the other hand, a variably spaced superlattice structure was designed to enhance the resonant tunneling between adjacent wells after the method reported [3, 14] and J-V characteristic

for this devices is obtained. The effect of the superlattice characteristics on the conversion efficiency is discussed. The SLSC conversion efficiency is compared with the maximum conversion efficiency obtained for the QWSC. Finally, we present GaAs/ GaInNAs SLSC conversion efficiency as a function of solar concentration, showing an clear increment in its performance.

2. Model details

In this section, we will develop the model, starting with the QWSC, whose structure is shown in figure 1. The make use of the common assumptions of homogeneous composition in the doped and intrinsic layers, the depletion approximation in the space-charge region, and total photogenerated carrier collection, assuming an equal carrier temperature in all regions. Transport and Poisson equations were used to compute the quantum efficiency in the charge-neutral layers while the quantum efficiency of the intrinsic region is determined taking into account the absorption coefficient of the nanostructure involved. The overall photocurrent is simply expressed in terms of superposition, adding photocurrent, obtained form the calculated quantum efficiency, to the dark current in order to find out the illuminated current-voltage characteristic.

2.1. Modelling the Quantum Well Solar Cell

The derived current-voltage relationship of a QWSC with N_W wells each of length L_W into the intrinsic region of length W, with barrier band gap Eg_B and well band gap Eg_W is given by equation 1, after [15, 16];

$$J(V) = J_0(1 + r_R\beta)\Big[\exp(\frac{qV}{\mathbf{k_B}T}) - 1\Big] + (\alpha r_{NR} + J_S)\Big[\exp(\frac{qV}{2\mathbf{k_B}T}) - 1\Big] - J_{PH} \tag{1}$$

where q is the electron charge, V is the terminal voltage of the device, $\mathbf{k_B}T$ the thermal energy, $\alpha = qWA_Bn_{iB}$ and $\beta = \frac{qWB_Bn_{iB}^2}{J_0}$ are parameters defined following Anderson [17]. J_0 is the reverse saturation current density; A_B is the nonradiative coefficient for barriers in the depletion region, which is related to barrier non-radiative lifetime τ_B by $A_B = \frac{1}{\tau_B}$; B_B is the radiative recombination coefficient of the host material; n_{iB} is the equilibrium intrinsic carrier concentration for the host material; r_R and r_{NR} are the radiative enhancement ratio and non-radiative enhancement ratio respectively given by the equations 2 and 3.

$$r_R = 1 + f_W\left[\gamma_B\gamma_{DOS}^2\exp\left(\frac{\Delta E - qFz}{\mathbf{k_B}T}\right) - 1\right] \tag{2}$$

$$r_{NR} = 1 + f_W\left[\gamma_A\gamma_{DOS}\exp\left(\frac{\Delta E - qFz}{2\mathbf{k_B}T}\right) - 1\right] \tag{3}$$

Those enhancement ratios represent the fractional increase in radiative and non-radiative recombination in the intrinsic region, due to the influence of quantum wells. In the

http://dx.doi.org/10.5772/59616

equations 2 and 3, $\Delta E = Eg_B - Eg_W$, f_W is the fraction of the intrinsic region volume substituted by the quantum well material, $\gamma_{DOS} = \frac{g_W}{g_B}$ is the density of states enhancement factor, g_W and g_B are the effective density of states for the wells and barriers, and γ_B and γ_A are "oscillator enhancement factor" and "lifetime reduction factor", respectively [17]. The built-in field is denoted by F and z is the position in the wells, so r_R and r_{NR} are position dependent. The photocurrent J_{PH} is calculated from the quantum efficiency of the cell. The p-region and n-region contribution to QE was classically evaluated solving the carrier transport equations at room temperature within the minority carrier and depletion approximations. The quantum efficiency (QE) is calculated by the expression:

$$QE(\lambda) = [1 - R(\lambda)] \exp\left(-\sum_{i=1}^{3} \alpha_i z_i\right) [1 - \exp(-\alpha_B W - N_W \alpha_W^*)] \tag{4}$$

where $R(\lambda)$ is the surface reflectivity of the antireflection layer. The first exponential factor is due to the attenuation of light in the precedent layers to the depletion layer as showed in Figure 1. The layers numbered in Figure 1, are: (1) antireflection coating, (2) emitter and (3) space-charge region of the emitter; α_i is the the absorption coefficient of each layer and z_i its corresponding width, α_B is the absorption coefficient of the bulk barrier material, and α_W^* is the dimensionless quantum well absorption coefficient, used for energies below the barrier band gap.

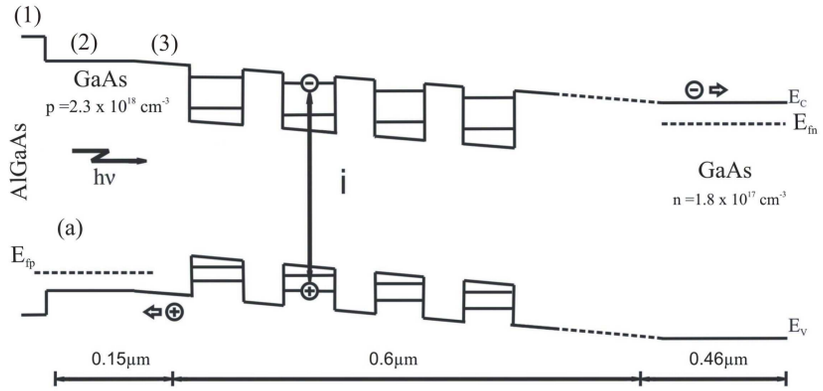

Figure 1. Sketch of energy band diagram of a GaAs p-i-n solar cell with quantum wells inserted within the intrinsic region.

When mixing between light and heavy valence sub-bands is neglected, the absorption coefficient can be calculated as follows[18]

$$\alpha_W^* = \alpha_W \Lambda \tag{5}$$

$$\alpha_W(E) = \sum \alpha_{e_n - hh_m}(E) + \sum \alpha_{e_n - lh_m}(E) \tag{6}$$

where $\sum \alpha_{e_n - hh_m}(E)$ and $\sum \alpha_{e_n - lh_m}(E)$ are sums over well states n and m, which numbers depend on the quantum wells width and depth, $\alpha_{e_n - hh_m}(E)$ and $\alpha_{e_n - lh_m}(E)$ are the absorption coefficients due to electron-heavy hole and electron-light hole transitions to conduction band, respectively; α_W is the well layer absorption coefficient and Λ is called "quantum thickness of the heterostructure" [18].

The exciton absorption is taken into account in the theoretical calculation and exciton binding energies are analytically evaluated in the framework of fractional-dimensional space developed by Mathieu et al [19]. Once the total QE is calculated, by using the AM1.5 incident solar spectrum represented by $F(\lambda)$, the photocurrent is then determined by integration following equation 7:

$$J_{PH} = q \int_{\lambda_1}^{\lambda_2} F(\lambda) QE_{TOTAL}(\lambda) d\lambda \tag{7}$$

where λ_1 and λ_2 are limits of the taken solar spectrum. Then, equation (1) is completely determined and conversion efficiency η can be evaluated.

2.1.1. Including the effect of strain in the nanostructure of QWSC

As mentioned previously, the best host material for a QWSC should be GaAs. However is very difficult to grow high quality quantum wells in a GaAs p-i-n solar cell because there are no high quality, lattice matched materials with a lower band-gap than GaAS. Therefore is required to use strained materials for that goal, but, once a critical thickness of strained material is deposited, it relaxes and causes the formation of misfit dislocations, which serve as centres for non-radiative recombination [20].

The increase in average strain can be limited by including tensile and compressively strained layers alternatively, choosing appropriately alloy composition and layer thickness, and taking into account each elastic constant. This way is possible to obtain structures which are locally strained, but exert no net force on the substrate or neighbouring repeat units. Such strain-balanced structures have demonstrated great photovoltaic performance, and the strain-balanced quantum well solar cell (SB-QWSC) is currently the most efficient QWSC [21].

One of the methods to reach the strain balance condition is the average lattice method [22]. If we considered L_B as the barrier thickness, L_W as the well thickness, and we denote a_B and a_W as the respective well and barrier lattice constants; its defined as:

$$a_{GaAs} \equiv \langle a \rangle = \frac{L_B a_B + L_W a_W}{L_B + L_W} \tag{8}$$

The total strain in the layer may be separated into a hydrostatic component and an axial component. In the case of unstrained bulk material, the heavy hole (hh) and light hole (lh) bands are degenerate at the Brillouin zone centre. The hydrostatic component of strain acts on the band edges changing the band gaps. On the other hand, the axial strain component acts on degeneration of bands. In the valence band, the axial component broken the degeneracy that exists at the band edge (Γ point).

Under compressive strain, the bottom energy of the conduction band is shifted to higher energies and the valence band splits, with the light hole band moving further away from the conduction band than the heavy hole band, suppressing the lh transition [23]. In contrast, under tensile strain the material band gap is reduced and the higher energy valence band is the light hole band.

During strained growth, the lattice constant of the epitaxial layer is forced to be equal to the lattice constant of the substrate. Then, there is an biaxial in-plane strain $\varepsilon_{i,j}$, where i, j = x, y, z. In the case of biaxial strain in (001) plane, the values along [001] direction are $\varepsilon_{xx} = \varepsilon_{yy} \neq \varepsilon_{zz}$. The strain causes changes of the band edges as explained above at Γ point, which are given by [24]:

$$E^{\varepsilon}_{hh} = a_v(2e_{xx} + e_{zz}) - b(e_{xx} - e_{zz}) \tag{9}$$

$$E^{\varepsilon}_{lh} = a_v(2e_{xx} + e_{zz}) + b(e_{xx} - e_{zz}) - b^2\frac{(e_{xx} - e_{zz})^2}{\Delta_{SO}} \tag{10}$$

$$E^{\varepsilon}_{c} = Eg + a_c(\varepsilon_{xx} + \varepsilon_{yy} + \varepsilon_{zz}) \tag{11}$$

where E^{ε}_{hh}, E^{ε}_{lh} and E^{ε}_{c} are the energy level values under strain for heavy holes, light holes and electrons, respectively, Eg is the band gap, a_v and a_c are the hydrostatic deformation potentials, b is the shear deformation potential and Δ_{SO} is the spin-orbit splitting of the valence band at Γ point. The separation of the total hydrostatic deformation potential in conduction (a_c) and valence band (a_v) contributions is important at heterointerfaces.

The band structure dispersion relations for strained InGaAs and GaAsP, are shown in Figure 8. Note that due to strains, the $In_{0.2}Ga_{0.8}As$ layer experiences a band increment of 121 meV, while for $GaAs_{0.7}P_{0.3}$ layer a decrease up to 176 meV is obtained. When the In and P compositions and layer widths are changed, such that the condition given by the definition (8) is satisfied, the strain is changed in the well and barrier layers, causing in both layers a variation in the absorption threshold.

The envelope function approximation is here assumed to determine QW energy levels in the conduction band. The electron energy E_e and wave function ψ_e can be then calculated within effective mass approximation. Then, the shift of the conduction band electron in the QW is described by Schrödinger equation. In order to obtain the QW energy levels in the hh and lh bands under varying compressive strain, a 4×4 $k \cdot p$ Kohn-Luttinger Hamiltonian was used:

$$H^{\varepsilon}_{KL} = H_{KL} + H^{\varepsilon} \tag{12}$$

where H_{KL} is the Kohn-Luttinger Hamiltonian without strain and H^{ε} is the strain Hamiltonian for epilayers grown in [001] direction, which is given by:

$$H^{\varepsilon} = \begin{bmatrix} E^{\varepsilon}_{hh} & 0 & 0 & 0 \\ 0 & E^{\varepsilon}_{lh} & 0 & 0 \\ 0 & 0 & E^{\varepsilon}_{lh} & 0 \\ 0 & 0 & 0 & E^{\varepsilon}_{hh} \end{bmatrix} \tag{13}$$

In a QW system, some splitting of the confined valence band levels takes place due to the differences in effective mass, which can be greatly enhanced if the QW is strained. When the well material is strained we have the confinement effects, but in addition we have the consequences of the non-degenerate bulk band edges. For example under (001) biaxial compressive strain the lh band is shifted further energetically from the conduction band.

In a sense, compressive strain acts in the same way as the effect of confinement. Then, biaxial strain, in well and barriers layers, lifts the degeneracy in the valence band such that it is possible to consider independently the hh and lh bands. Under above approximations, the QW energy levels for hh and lh bands where found. The Schrödinger equation corresponding to Hamiltonian is not separated so it is assumed that the "off-diagonal" terms, which lead to valence band mixing, are small enough that they can be neglected. With this assumption the Schrödinger equation becomes separable:

$$\left[-\frac{h^2}{2m_0}\left(\gamma_1 - 2\gamma_2\right)\frac{d^2}{dz^2} + U(z) + E_{hh}^{\varepsilon} - E_{hh}\right]\Psi_{hh}^{\uparrow}(z) = 0 \tag{14}$$

$$\left[-\frac{h^2}{2m_0}\left(\gamma_1 + 2\gamma_2\right)\frac{d^2}{dz^2} + U(z) + E_{lh}^{\varepsilon} - E_{lh}\right]\Psi_{lh}^{\uparrow}(z) = 0 \tag{15}$$

where $\Psi_{hh}^{\uparrow}$ and $\Psi_{lh}^{\uparrow}$ are the envelope functions with spin direction. The equations (14) and (15) are solved in barrier and well regions with the corresponding $U(z)$ potential and Konh-Luttinger parameter values (γ_1 and γ_2) in each layer. Computed the E_e, E_{hh} and E_{lh} values the optical transitions are calculated by Fermi's golden rule and the equation (7) is evaluated to determine the absorption in the quantum wells. Then, the procedure to calculate the photocurrent is analogous to that described in 2.1.

Compressive strain results in lower thermal occupancy of the *lh* band relative to the *hh* band, and radiative transitions from the conduction to the *hh* band are favored over those to the *lh* band. If the splitting becomes greater than a few $\mathbf{k_B}T$, *lh* transitions could be suppressed almost entirely[23]. In order to examine this behavior, the anisotropic radiative recombination and gain, as consequence of the strain in the quantum wells, is investigated in order to determinate their influence in the SB-QWSC performance.

As a result of the dislocation-free material, the radiative recombination dominates in SB-QWSCs at high current levels bringing the structure close to the radiative limit. This allows the exploitation of radiative photon recycling by means of the growth of distributed Bragg reflectors (DBRs) between the active region and the substrate of the cell, increasing the efficiency of the SB-QWSC.

This observed increase in solar cell efficiency due to DBRs is due to first to the reduction of the dark current via radiative photon recycling, and second to an increase in photocurrent. The first is due to the reflection of radiative emission back into the cell, reducing the net radiative emission and there-fore, the radiative dark current which, as we have seen, dominates in these structures. The second is the product of the reflection of photons back into the cell of photons which would otherwise have been absorbed in the substrate, leading

http://dx.doi.org/10.5772/59616

to decreased photon loss to the substrate, and increasing the photocurrent, equivalent to a net increase in the quantum well absorption.

We will discuss the theoretical background to radiative recombination, gain and photon recycling. The electron and hole quasi-Fermi separation was calculated in order to determine the spontaneous TE and TM emission rate from QW and gain as a function of In composition. Similarly, the optical transitions in quantum well are evaluated to calculate the QW absorption coefficient. Then, we present the results of simulations of the SB-QWSC that it takes account of DBR and anisotropic effects. We calculate quantum and conversion efficiencies and observe an increment in the SB-QWSC performance, particularly under solar concentration.

The radiative recombination current could be suppressed in SB-QWSC devices with deep QWs relative to the prediction of the generalized Planck formula assuming isotropic emission. Following Adams et al [23], emission can be defined as TE, which is polarized in the plane of the QWs, and TM, which is polarized perpendicular to the plane of the QWs. It is therefore possible for TE-polarized light to be emitted either out of the face or the edge of the QWs, whereas TM polarized light can only be emitted out of the edge of the QWs. The *hh* transition couples solely to TE-polarized emission, and the lh band couples predominantly to TM-polarized emission with a minor TE-polarized contribution.

The spontaneous emission rates, R_{spon}, were calculated by ab-initio methods, where the transition from bulk to quantum wells structures was carried out by converting the 3D density of states to the 2D density states. Calculations of TE and TM emission out of the faces and edges of a quantum well include the strain modifications to the spontaneous emission rate resulting from varying the In and P compositions and their layer widths such that the condition given by equation (8) is satisfied.

The emission spectrum from a solar cell depends on the absorption coefficient and the carrier density through the quasi-Fermi-level separation, ΔE_f. To model the emission from either sample at a given generated strain, we first calculated the absorption coefficient using a quantum-mechanical model above mentioned. We assumed that the number of photogenerated carrier pairs is equal to the total emitted photo flux. In the absence of any photon density, the emission rate is the spontaneous emission rate, provided a state $\overrightarrow{k}$ is occupied by an electron and a hole is present in the same state $\overrightarrow{k}$ in the valence band. The rate depends on the occupation probability functions for electrons, f_e, and holes, f_h, with the same $\mathbf{k_B}$-value. The occupation probability function for electrons and holes depends on the corresponding quasi-Fermi level. The spontaneous emission rate expression for quantum well structures is obtained be integration over all possible electronic states

$$R_{spon} = \int d(\hbar\omega) A\hbar\omega \sum_{n,m} \left[\frac{d^2k}{(2\pi)^2} |\widehat{a} \cdot \overrightarrow{p}_{if}|^2 \delta \left(E_n^e(\overrightarrow{k}) - E_m^h(\overrightarrow{k}) \right) \times f_e(E_n^e(\overrightarrow{k})) f_h(E_m^h(\overrightarrow{k})) \right] \tag{16}$$

The integral over $d(\hbar\omega)$ is to find the rate for all photon emitted and the integration over d^2k is to get the rate for all the occupied electron and hole subband state. Equation (16) summarizes the discrete energy states of the electrons (index n) and the heavy holes (index

m) in the well. $E_n^e(\,k^{'}\,)$ and $E_m^h(\,k^{'}\,)$ denote the QW subbands of the electrons and heavy holes and δ denotes the Dirac delta function. The factor $A = \dfrac{2q^2 n_r}{m_0^2 c^3 h^2}$ is a material dependent constant, where n_r is the refractive index of the well material. The first term inside the element $|\widehat{a} \cdot \overrightarrow{p}_{if}|$ represents the polarization unit vector, $\widehat{a}$, while the second term represents the momentum matrix element, $\overrightarrow{p}_{if}$. The spontaneous emission rate of the QWs was calculated using the above formula.

In a semiconductor in nonequilibrium condition, the total electron concentration n and the total hole concentration p are described to be the, respectively, electron and hole quasi-Fermi levels. If detailed balance is applied when each photon produces one electron-hole pair and all recombination events produce one photon, the electrons and hole quasi-Fermi levels in the quantum well structure were calculated by solving the following system of equations [28]:

$$n(E_{F_c}) = p(E_{F_h}); \qquad \Delta E_f = E_{F_c} - E_{F_h} \tag{17}$$

Determining ΔE_f is essentially a matter of normalizing the emission spectrum to the generation rate. If detailed balance applies, the number of photogenerated carrier pairs is equal to the total emitted photon flux, and the gain (G) is defined is defined as the number of photogenerated carrier pairs per unit area and time:

$$G = \iint_0^\infty G(\lambda, z) dz d\lambda = \int_0^\infty L(\hbar\omega) d(\hbar\omega) \tag{18}$$

where $G(\lambda, z)$ is the electron-hole pair generation rate at z depth from the surface in the growth direction and is given by the expression:

$$G(\lambda, z) = [1 - R(\lambda)]\, \alpha(\lambda, z) F(\lambda) \exp\left[- \int_0^z \alpha(\hbar\omega, z') dz' \right] \tag{19}$$

The exponential factor is due to the attenuation of light in the layers between the surface of the cell and the depletion layer. The layers considered in our calculus are antireflection layer, emitter layer, and space-charge region from to the emitter layer (see Figure 7). The emitted flux density $L(\hbar\omega)$, of photons of energy $\hbar\omega$, is given by:

$$L(\hbar\omega) = \frac{2n_r^2}{h^3 c^2} \frac{\alpha(\hbar\omega)(\hbar\omega)}{e^{\frac{\hbar\omega - \Delta E_f}{\mathbf{k_B} T}} - 1} \tag{20}$$

At low enough carrier density, where ΔE_f is much smaller than the effective band gap, the Boltzmann approximation is used, and Eq. (20) is simplified, then the dependence on ΔE_f is an explicit function. From Eqs. 18 and 20, we found:

http://dx.doi.org/10.5772/59616

$$\Delta E_f = -\mathbf{k_B} T \ln \left[\frac{1}{G} \int_0^{\infty} \frac{2n_r^2}{(2\pi\hbar)^3 c^2} \alpha(\hbar\omega)(\hbar\omega)^2 \exp -\frac{\hbar\omega}{\mathbf{k_B} T} d(\hbar\omega) \right] \tag{21}$$

The total electron concentration is determined by:

$$n = \int_{E_{We}}^{E_{Be}} g_e^{QW}(E) f_e(E) dE + \int_{E_{Be}}^{\infty} g_e^{Bulk}(E) f_e(E) dE \tag{22}$$

where E_{W_e} and E_{B_e} are the conduction valence band edge energy for quantum well and barrier material respectively, $g_e^{QW}(E)$ is the electron quantum well density of state and $g_e^{Bulk}(E)$ is the electron bulk density of state in the quantum well material. The calculation of the total hole concentration is analogous. Then the equation system (17) may be solved and the quasi-Fermi level is determined. The spontaneous emission rate from QW region was then calculated according to Eq. (16).

2.2. Modelling the Superlattice Solar Cell

In contrast with a QWSC where the different quantum wells are considered independent and there is no coupling between neighboring quantum wells, in the superlattice solar cell an interaction exist between neighboring wells and the wave function becomes extended over the whole nanostructure. Therefore the discrete levels in isolated quantum wells spread into a miniband, as it can be seen in Figure 2.

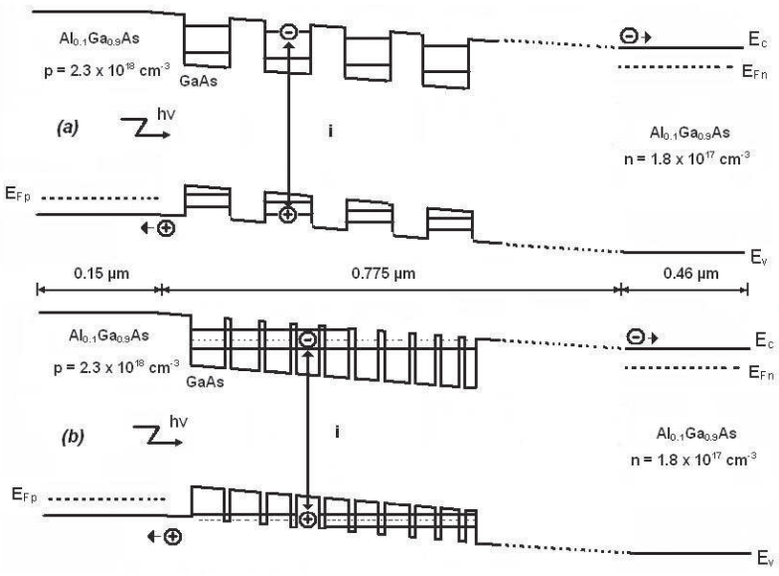

Figure 2. Sketch of energy band diagram of a typical $Al_{0.1}Ga_{0.9}As$ p-i-n solar cell with inserted quantum wells (a) and superlattices (b) in the intrinsic region

In order to achieve the quantum well coupling in the intrinsic region, which is inside an electric field, a variable spaced superlattice is proposed. In this case is necessary that each well width changes in the way that electron levels of the wells are resonant at the operating bias. Then the conditions are fullfilled for resonant tunneling of carriers in the whole nanostructure for a specific value of the electric field, which depends of the doping of the p- and n- regions.

From the theoretical point of view, the advantages of an SLSC over an QWSC are the following: (i) provides quantum levels for electrons and holes within specific eigen-energies (minibands), (ii) improves the miniband photon absorption, (iii) cancels deep-level recombination between single and double heterojunction, (iv) the carriers are able of tunneling along the growth direction through thin barriers while they are essentially free along the transverse direction, and (v) allows an efficient escape rate of carriers out of quantum wells, which are collected in the emitter and base regions [25].

In order to extend the model to the SLSC, the coefficients r_R and r_{NR} (Eqs. (2) and (3)) and the photocurrent J_{PH} should be related to superlattice structure. Now, the f_W factor is the intrinsic region fraction replaced by superlattices, with g_{SL} and g_B as the effective density of states for superlattices and barriers, $\gamma_B = B_{SL}/B_B$ and $\gamma_A = A_{SL}/A_B$ are the radiative and non radiative recombination coefficients referred to superlattices and barriers respectively. The photocurrent is evaluated using absorption coefficients of the transitions of the minibands. The effective density of states for electrons in the superlattice was found [3]:

$$\begin{aligned} g_{SLe} = & \frac{m_e}{\pi\hbar^2 d_{SL}} \int_0^{\Gamma_e} \left(\frac{1}{2} + \frac{1}{2} \arcsin\left(\frac{E - \frac{\Gamma_e}{2}}{\frac{\Gamma_e}{2}} \right) \right) \exp\left(-\frac{E + E_e}{\mathbf{k_B} T} \right) dE \\ & + \frac{m_e}{\pi\hbar^2 d_{SL}} \mathbf{k_B} T \left[\exp\left(-\frac{E_e + \Gamma_e}{\mathbf{k_B} T} \right) - \exp\left(-\frac{\Delta E_c}{\mathbf{k_B} T} \right) \right] \\ & + 2 \left(\frac{2\pi m_e \mathbf{k_B} T}{\hbar^2} \right)^{\frac{3}{2}} \left[2\sqrt{\frac{\Delta E_c}{\pi \mathbf{k_B} T}} \exp\left(-\frac{\Delta E_c}{\mathbf{k_B} T} \right) + erfc\sqrt{\frac{\Delta E_c}{\mathbf{k_B} T}} \right] \end{aligned} \tag{23}$$

where E_e is the electron miniband bottom, $erfc$ is the complementary error function, m_e is the electron effective mass, $\Delta E_c = Q_c(Eg_B - Eg_W)$ is the well depth in the conduction band, Q_c is the band offset factor, d_{SL} is the superlattice period and Γ_e is the miniband width in the conduction band. Analogous expressions are obtained for heavy hole and light hole effective density of states ($g_{SL_{hh}}, g_{SL_{lh}}$). Then the total superlattice effective density of states was calculated as:

$$g_{SL} = \sqrt{g_{SLe}(g_{SL_{hh}} + g_{SL_{lh}})} \tag{24}$$

The absorption coefficient for the transitions between light hole and electron minibands was also determined as a function of their widths, Γ_{lh} and Γ_e which we will use in our model as

http://dx.doi.org/10.5772/59616

a parameter:

$$\alpha_{lh-e}(E) = \frac{q^2}{cm_e^2\varepsilon_0 n_r d_{SL}\hbar^2\omega}|\hat{a}\cdot\overrightarrow{p}_{if}|^2 \times \frac{m_{lh}m_e}{m_{lh}+m_e}\left\{\frac{1}{2}+\frac{1}{\pi}\arcsin\left[\frac{E-Eg_0-\frac{\Gamma_e+\Gamma_{lh}}{2}}{\frac{\Gamma_e+\Gamma_{lh}}{2}}\right]\right\} \quad (25)$$

where $|\hat{a}\cdot\overrightarrow{p}_{if}|$ is the optical matrix element between the initial i and the final f transition states, a is an unit vector in the direction of propagation, p is the momentum, n_r is refraction index of the heterostructure, ε_0 is the vacuum dielectric constant, ω is the angular frequency of radiation, m_{lh} is the light hole effective mass, $Eg_0 = Eg_W + E_e + E_{lh}$ and E_{lh} is the light hole miniband top energy. An analogous expression for the absorption coefficient of the transitions between heavy hole and electron minibands ($\alpha_{hh-e}(E)$) is also found. The total superlattice absorption coefficient can be expressed by:

$$\alpha(E) = \alpha_{lh-e}(E) + \alpha_{hh-e}(E) \quad (26)$$

According to the detailed balance theory, the radiative recombination coefficient is expressed by:

$$B = \frac{8\pi n_r^2}{c^2h^3n_0p_0}\int_{E_1}^{E_2}\frac{\alpha_{SL}E^2dE}{\exp\left(\frac{E}{\mathbf{k_B}T}\right)-1} \quad (27)$$

Now the quantum efficiency the intrinsic region is calculated by the expression 28, considering the absorption of photons through a miniband and not by quantum well levels:

$$QE(\lambda) = [1-R(\lambda)]\exp\left(-\sum_{i=1}^{3}\alpha_i z_i\right)[1-\exp\left(-\alpha_B W - N_{SL}L_{SL}\alpha_{SL}^*\right)] \quad (28)$$

where L_{SL} is the superlattice width. This superlattice could be considered an structural unit and we can repeat several of this superlattice units as much as they fit inside the intrinsic region. So, let's define this superlattice units as a cluster. Then, N_{SL} is the number of clusters or superlattice units that we insert in the intrinsic region of the p-i-n solar cell.

Once the expressions for the effective density of states, the absorption coefficient, the radiative recombination coefficient, and photocurrent were found for SLSC, we are able to determine the J-V characteristic from equation (1) and then it is possible to calculate the conversion efficiency.

3. Results and Discussion

3.1. AlGaAs/GaAs multiple quantum well and superlattice solar cell

As a test of our model, we compare the QE calculated with the experimental values of G951 QWSC sample ($Al_{0.33}Ga_{0.67}As/GaAs$) from the Quantum Photovoltaics Group at Imperial College London [26]. Table 1 displays the pertinent features of several solar cells that were

used to compare our model with experimental parameters. The absorption coefficient of $Al_xGa_{1-x}As$ bulk solar cell was determined from the GaAs spectrum $\alpha(\lambda)$, using the same nonlinear shift of the energy axis reported by M. Paxman et al. [5].

The expressions for the generation of the bulk absorption coefficient and the values of AlGaAs parameters used in the calculation are obtained from reference [15]. The internal quantum efficiency for G951 QWSC is calculated as function of energy and is compared to experimental curve shown in Figure 3, where is shown a good agreement between experimental and modeled spectra. In the calculations only the QWSC growth and material parameters were used, without any fitting parameter. The deconvolved spectra in Figure 3 clearly show that the absorption edge of the QWSC is shifted to lower energies due to the existence of quantum wells in the intrinsic region, and increases the QE values in the short wavelength region and consequently the short-circuit current will increase.

Cell	Cap (μm)	p layer (μm)	p doping (cm^{-3})	n layer (μm)	n doping (cm^{-3})	i layer (μm)	well number	well width (μm)
G946	0.017	0.15	1.3×10^{18}	0.46	1.3×10^{18}	0.51	50	8.5
QT76	0.02	0.3	7.0×10^{17}	0.6	3.0×10^{17}	0.48	30	8.7
G951	0.02	0.15	1.3×10^{18}	0.46	1.3×10^{18}	0.81	50	8.5
QT468A	0.04	0.15	9.0×10^{17}	0.6	2.5×10^{17}	0.48	30	8.4
QT229	0.045	0.5	2.0×10^{18}	0.5	6.0×10^{18}	0.80	50	10.0
QT468B	0.02	0.15	9.0×10^{17}	0.6	2.5×10^{17}	0.48	0	0
CB501	0.02	0.15	9.0×10^{17}	0.6	9.0×10^{17}	0.31	1	5.0

Table 1. Details of cells structures

Good fit between modeled and experimental QE spectra was also observed for all solar cells reported in Table 1. The photocurrent calculated by equation (7) is compared with the experimental values in Table 2 and also show good agreement as the difference between theoretical and experimental values did not exceed 10%.

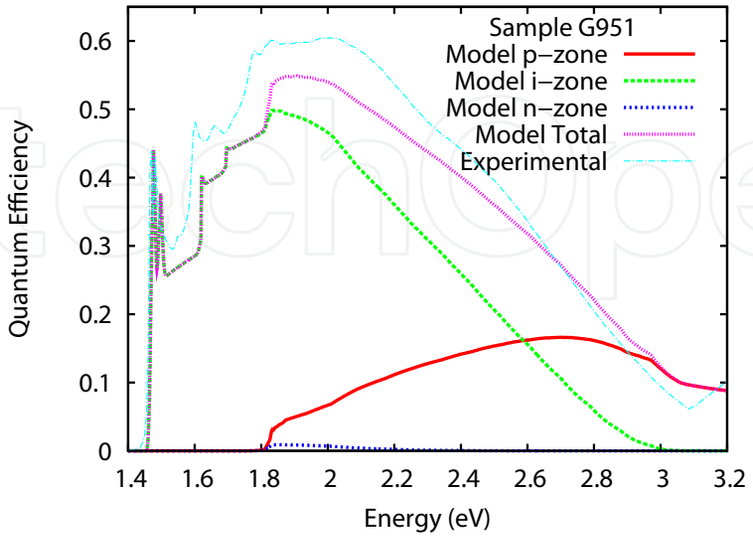

Figure 3. Experimental and modeled IQE for G9551 QWSC. The contributions from p, i, and n layers are separated.

http://dx.doi.org/10.5772/59616

We also compared the calculated open-circuit voltages with experimental shown in table 3 for four QWSCs, showing a good agreement between experimental and calculated values.

The influence of the quantum well width and the barrier band gap energy upon the normalized efficiency η^* is shown in Figure 4. We define the η^* as the ratio between $Al_xGa_{1-x}As/GAs$ QWSC efficiency and baseline p-i-n solar cell efficiency. The best values for η^* are obtained for shallow and wider wells with an efficiency enhancement of about 15%. Increasing the quantum well thickness also increases the normalized efficiency until saturation. For high barrier Al concentration the normalized efficiency grows more quickly with the increase of L_W. The η^* have a maximum value for 15 wells of 15 nm width using $Al_{0.1}Ga_{0.9}As/GaAs$ QWSC, with and approximately 20% of efficiency enhancement between the QWSC and its equivalent baseline cell. On the other hand, the increase of Al composition in the barrier, that means deeper wells, is detrimental for η^*.

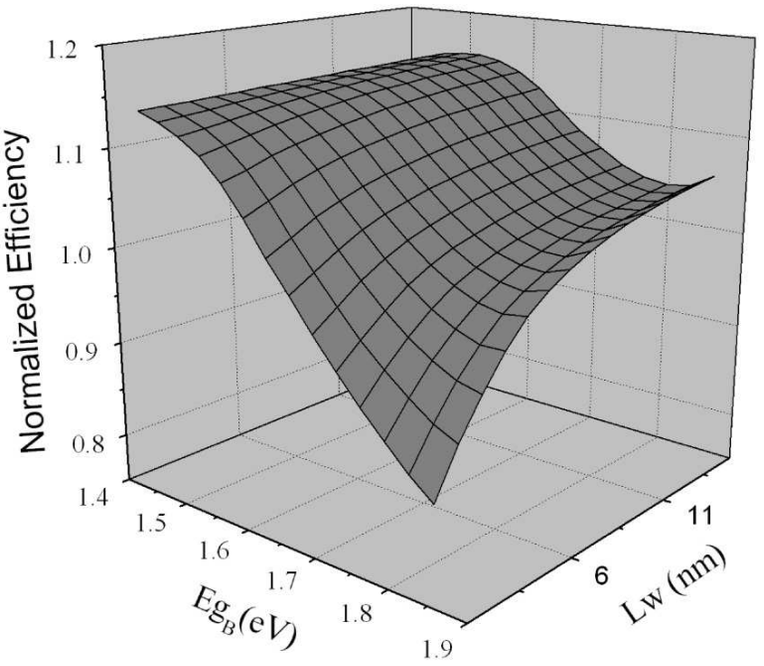

Figure 4. AlGaAs/GaAs QWSC normalized efficiency as a function of the quantum well width and the barrier band gap energy for $N_W = 20$.

On the other hand, the expected high efficiency of the SLSC not only depends on the material and structure quality, ensuring minimum non-radiative recombination losses at the bulk and the interfaces, but it also depends on the escape rate of photogenerated carriers out of the clusters into the n and p-regions having minimum radiative losses within minibands.

We looked for recombination mechanisms in an SLSC and compared them with the same mechanisms in an QWSC. Using Equations (2)-(3) , we calculated radiative enhancement ratio, non-radiative enhancement ratio, and the interface recombination current for the SLSC (Figure 2(b)). These coefficients are function of the effective density of states and the absorption coefficient, which depend on the electron miniband width. Similar calculations were carried out for an QWSC with 15-nm well width and 24 wells in the intrinsic region (Figure 2(a)) where the efficiency reaches a maximum, which is always higher to the

corresponding homogeneous p-i-n cell without quantum wells, as it was shown in a previous study [3].

Sample	Photocurrent (A/m^2)	
	calculated	experimental
G946	87.8	82.2
QT76	76.0	81.5
G951	112.0	132.8
QT468A	76.8	77.0
QT229	18.9	20.6

Table 2. Experimental and calculated photocurrent of AlGaAs QWSCs.

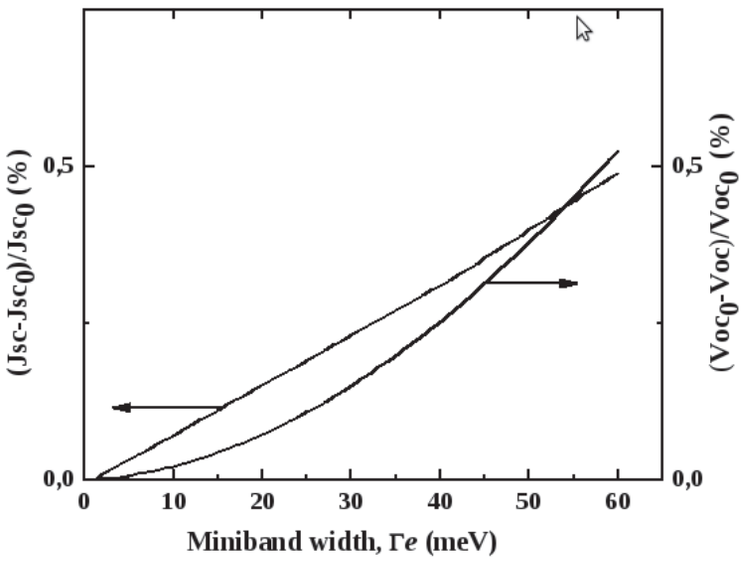

Figure 5. $(Jsc - Jsc_0)/Jsc_0$ and $(Voc_0 - Voc)/Voc_0$ as a function of electron miniband width. Jsc_0 and Voc_0 were calculated for Γe = 1 meV.

In the case of the AlGaAs/GaAs SLSC, the effective density of states and the absorption coefficient were calculated using the AlGaAs parameters reported in Table 2 of reference [15]. The short-circuit current density J_{SC} and the open-circuit voltage V_{OC} were determined using Equation (1) and showed in Figure 5, as a function of the miniband width Γ_e. In this figure, J_{sc_0} and V_{oc_0} were calculated at $\Gamma_e = 1meV$ and it can be observed that an increment in the electron miniband width causes a light increase in the J_{sc_0} and the V_{oc_0} does not decrease significantly. This result suggests that changing the width of the miniband does not influence

Sample	$V_{OC}(V)$	$V_{OC}(V)$
	experiment	theory
QT468A	0.99	0.99
QT229	1.02	0.97
CB501	1.10	1.16
QT468B	1.18	1.28

Table 3. Experimental and calculated open-circuit voltage for three AlGaAs QWSCs.

http://dx.doi.org/10.5772/59616

too much the photon absorption, which could be because solar photon density in that spectral region is not high. The linear dependence of J_{SC} is a confirmation of this assumption. The very small decrease in V_{OC} is a consequence of the weak increment of the interface recombination current with the miniband width.

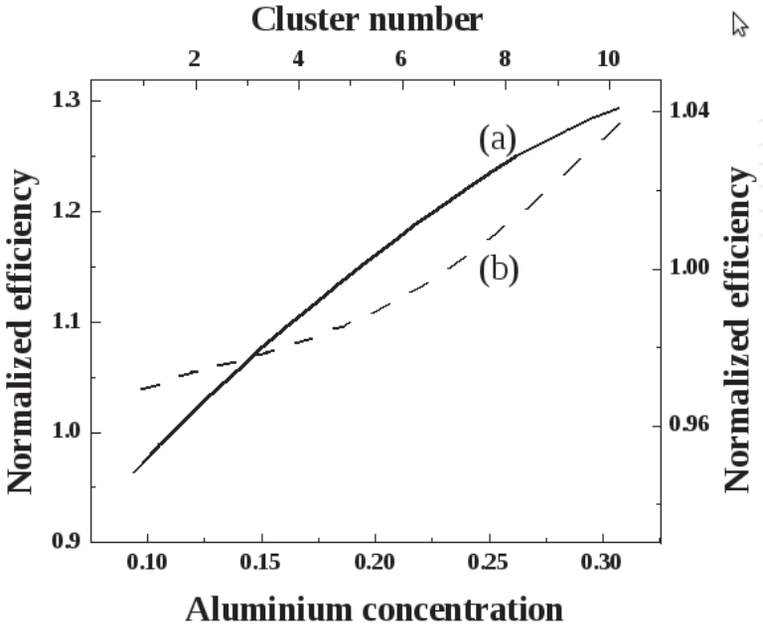

Figure 6. The normalized efficiency versus cluster number (a) and Al composition (b). The normalized efficiency is defined as the ratio between SLCS efficiency and its equivalent QWSC efficiency

If we increase the electric field in the intrinsic region, the number of quantum wells in the superlattice period should be smaller in order to obtain the resonant tunneling conditions. Therefore, a larger amount of cluster should be inserted to enhance the absorption, but then the interfaces and non-radiative recombination will increase. Great reduction of the electric field is not good in the p-i-n solar cells because it requires a low doping level in the p- and n-regions or an increase of the intrinsic region width.

After aplying the model proposed to the case of AlGaAs/GaAs SLSC, it was obtained that the three studied recombination mechanisms show independence with electron miniband width, remaining constant the heavy and light-hole miniband width, 35 and 15 meV, respectively. This is a significant result because the photocurrent could be improved in SLSC, and open-circuit voltage does not change. The values of the SLSC radiative recombination are almost smaller by two orders of magnitude than those obtained for the QWSC.

This result suggests that photogenerated carriers can escape out of the clusters more efficiently in SL structures because transport of carriers is enhanced via tunneling through thin potential barriers. In fact, the electrons in the minibands have high probability of tunneling assisted by electric field, through thin barriers and are recollected in n-AlGaAs region. An advantage of an SL barrier over a bulk barrier is the elimination of deep-level recombination between single and double heterojunctions, therefore, a non-radiative recombination reduction is expected in SLSC. This assumption is supported by our calculations, which show a drop in the non-radiative recombination value. The interface recombination current is greater for SLSC as a consequence that there are more interfaces,

in particular, when 10 clusters of superlattices are inserted in the intrinsic region. Therefore, this mechanism becomes the most relevant for SLSC.

We researched the AlGaAs/GaAs SLSC efficiency, which was compared with the AlGaAs/GaAs QWSC efficiency. Figure 6 illustrates the normalized efficiency versus Aluminium composition and cluster number in the QWSC. The normalized efficiency in this figure is defined as the ratio between the efficiencies of SLSC and its corresponding QWSC for the graph versus Aluminium concentration. In the case of the graph in function of the cluster number the QWSC efficiency in the ratio is the highest. The SLSC efficiency is better than the highest QWSC efficiency for five or more clusters of superlattices in the intrinsic region which meas that under these conditions the photocarrier generation in the SLSC overcome the recombination. However, the best SLSC efficiency is just 4% better than the QWSC efficiency because the increase of SLSC photocurrent does not increase enough. This suggest that the miniband absorption and the absorption of wide quantum wells are comparable. On the other hand, normalized efficiency was plotted versus Al concentration in the QWSC, for 10 clusters in the SLSC intrinsic region, 15 nm well width, and 24 wells in the QWSC intrinsic region and in this case Figure 6 exhibits that SLSC efficiency is always higher than the QWSC efficiency, and become larger as the well barrier height increases. Because of the results that our model predictions are neither compared nor confirmed experimentally, it would be interesting to see if future experiments will corroborate our findings.

3.2. Strain-balanced GaAsP/InGaAs/GaAs SB-QWSC

The SB-QWSC is a GaAs p-i-n solar cell with quantum well layers incorporated into the i-region with InGaAs as well material and GaAsP as barrier material. Figure 7 shows the band-structure of the GaAsP/InGaAs/GaAs SB-QWSC modeled by C. I Cabrera et al. [27].

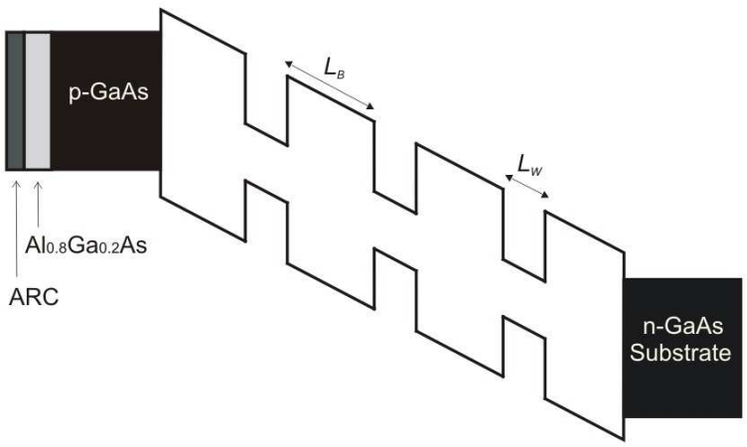

Figure 7. The band-structure of the SB-QWSC. The QW stack is embedded within the depletion zone of the GaAs cell and extends the absorption edge of the cell beyond that of a classical GaAs solar cell.

The compressive strain in the InGaAs QW is matched by tensile strain in GaAsP barriers, overcoming the lattice-mismatch limitation. The GaAsP and InGaAs layer widths were chosen to ensure the average lattice parameter across the i-region was equal to that of GaAs following equation 8, where the barrier material is GaAsP and well material InGaAs.

http://dx.doi.org/10.5772/59616

Elastic constants were considered to evaluate the tensile and compressive strain in GaAsP and InGaAs layers and examine the effect on the band structure of both materials under strain. Consequently, when the In an P compositions are varied, the strains in the barrier and well layers modify absorption threshold in both layers.

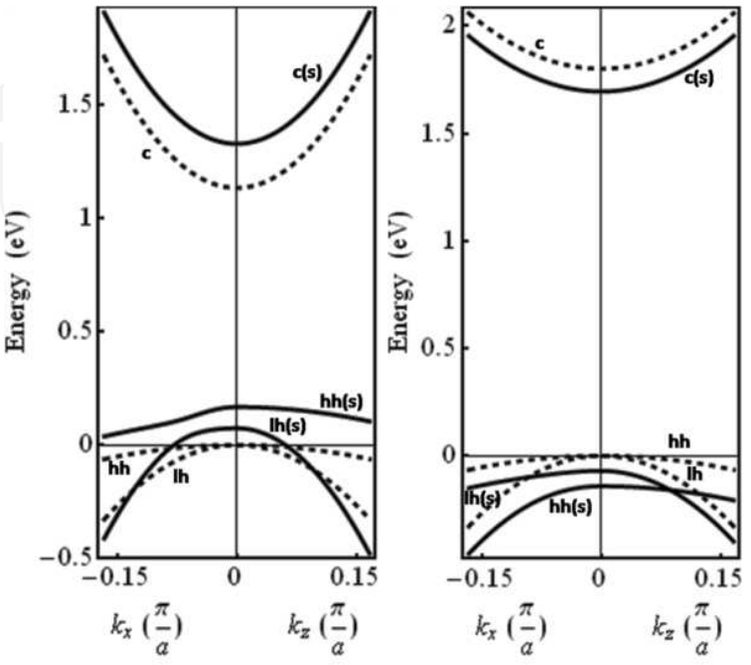

Figure 8. Representation of the effect of strain on band structure of $In_{0.2}Ga_{0.8}As$ and $GaAs_{0.7}P_{0.3}$ around of the first Brillouin zone center compared with unstrained bulk material (dashed line) which is degenerate degenerate at the zone centre for valence band. $c(s)$ is the strained conduction bands, $lh(s)$ and $hh(s)$ are the strained light and heavy hole bands, respectively (straight lines). The vertical axes give the energy in eV, the lateral axes give the wave number k_x and k_z, respectively. (a) Shift and deformation of $In_{0.2}Ga_{0.8}As$ energy bands for compressive strain, $\varepsilon_{xx} = -0.014$, $\varepsilon_{zz} = 0.013$, (b) of $GaAs_{0.7}P_{0.3}$ energy bands for tensile strain, $\varepsilon_{xx} = 0.019$; $\varepsilon_{zz} = -0.010$.

The p- and n- regions were designed with 200 and 500 nm width respectively, with a 40 nm $Al_{0.8}Ga_{0.2}As$ window layer before the p-region to reduce front surface recombination, with a MgF: SiN layerfor anti-reflective coating (ARC) of 70 nm width. The electron and hole concentrations are $n = 10^{18}cm^{-3}$ and $p = 10^{18}cm^{-3}$, respectively. Finally a passivation layer in the solar cell rear was assumed with 200 cm/s surface recombination velocity.

Figure 9 depicts TE and TM spontaneous emission rates and the ratio TM/TE as a function of In fraction. The discontinuous steps at approximately 6% In are due to the emergence of QW energy levels, $e_2 - hh_2$ and $e_2 - lh_2$ transitions as the well depth increases. It is evidenced that as the In fraction increases, the QWs influence a higher compressive strain. As a result of this, radiative transitions from the conduction band to *hh* band (TE) are favoured over those to *lh* band (TM). However, both polarized emissions increase with well depth, indicating that biaxial compressive strain does not suppresses a mode of radiative recombination in the plane of the QWs, although certainly the TM/TE ratio is reduced. We, consequently, observe that increasing the In composition leads to larger radiative recombination that increases the total recombination dark current.

In Figure 10, spontaneous emission rates and gain are presented as a function of In fraction, where is important emphasize the great difference between the values of the spontaneous

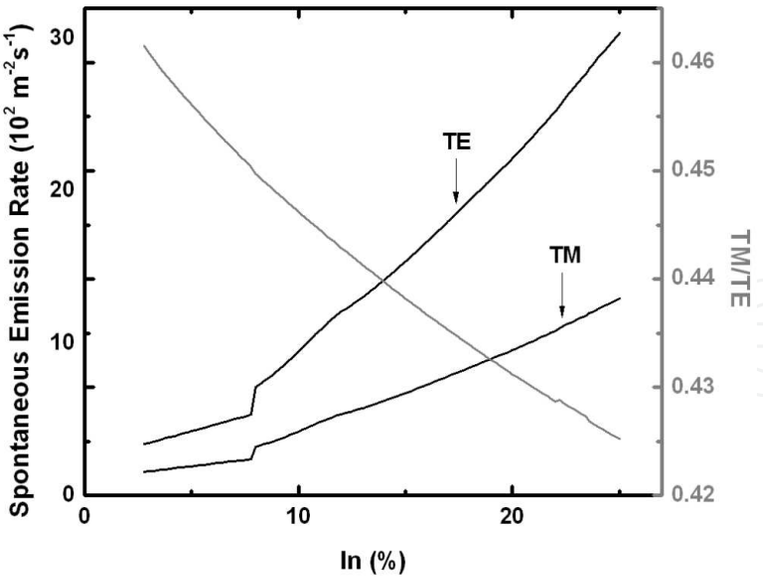

Figure 9. Modeled spontaneous emission rate for TE and TM modes and TM/TE ratio versus In composition for 10 well embedded within i-region of the SB-QWSC. Well width, L_W =15 nm and P composition, y = 0.05. The TE mode is favored over TM mode, but both polarized emissions increase with well depth.

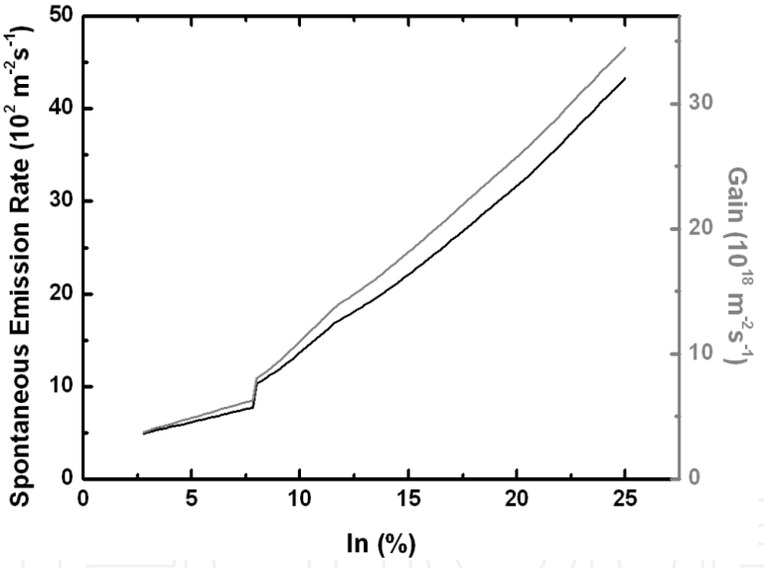

Figure 10. Spontaneous emission rate and gain versus In composition for 10 well embedded within i-region of the SB-QWSC. Well width, L_W =15 nm and P composition, y =0.05. Gain is several orders greater than radiative recombination

emission rates evidenced in the ratio TM/TE. The results of this study indicate that the generation of electron-hole pairs in the QWs is much higher than the radiative recombination, and if we add to this the influence of transverse electric field in the depletion region, which favors thermally assisted tunneling, then the carriers escape from the QWs with unity efficiency.

A distributed Bragg reflector (DBR) is a region consisting of layers of alternating refractive indices optimized for a specific wave-length such that each layer is a quarter wavelength

http://dx.doi.org/10.5772/59616

thick. As a result, partial reflections from each interface interfere constructively and the reflectivity is high over a narrow wavelength band.

Photon-recycling is the generation of an electron-hole pair via the absorption of a photon emitted elsewhere in the cell. The increased absorption is due to the reflection of incident solar radiation which has not been absorbed on its first pass through the cell and may then be reabsorbed on its second pass. It is equivalent to say that a DBR doubles the optical path length of a SB-QWSC without altering the length over which minority carriers must travel. The photons emitted by recombination into quantum wells were also considered.

The net solar incident radiation flow on front surface of a solar cell was modeled as a Fabry-Perot cavity. We derived an expression to calculate the contribution of the multiple internal reflections inside the device and then the net spectrum, $F_{net}(\lambda)$, which takes into account all contributions and the incident AM1.5 solar spectrum $F(\lambda)$ is given by:

$$F_{net}(\lambda) = F(\lambda)\left[1 + \frac{r_B\left(r_A + e^{\alpha_T^*}\right)}{e^{2\alpha_T^*} - r_B r_A}\right] \tag{29}$$

$$\alpha_T^* = \sum_j \alpha_j(\lambda) l_j \tag{30}$$

where $\alpha_j(\lambda)$ are the absorption coefficients of each layer of Fabry-Perot cavity structure, where the exciton effect in the quantum well was taken into account, l_j are layer widths, and r_A, r_B are the internal reflectivity from the front and back surface of the cell, respectively.

The photocurrent J_{PH} is calculated from the total quantum efficiency (QE_{TOTAL}) of the cell:

$$J_{PH} = q\int_{\lambda_1}^{\lambda_2} F(\lambda)\left[1 + \frac{r_B\left(r_A + e^{\alpha_T^*}\right)}{e^{2\alpha_T^*} - r_B r_A}\right] QE_{TOTAL}(\lambda)d\lambda \tag{31}$$

where $\lambda_1 = 400nm$ and λ_2 is the effective absorption threshold determined by the fundamental electron and hole confinement states.

Figure 11 shows modeled and experimental quantum efficiency (QE) versus wavelength for qt1897b sample from the Quantum photovoltaics Group of Imperial College. The cell is a p-i-n diode with an i-region containing five QWs that are 9.6 nm wide of compressively strained $In_{0.16}Ga_{0.84}As$ inserted into tensile-strained $GaAs_{0.91}P_{0.09}$ barriers at strain-balance condition. The extra absorption is displayed in the inset of Figure 11, at wavelengths in excess of the GaAs band gap where the increase in quantum efficiency in the 880 nm is readily apparent. Figure 11 also shows the computed QE spectrum with DBR, using $r_A = 0.1$ and $r_B = 0.95$. The main feature of this plot is that for a highly reflecting mirror, nearly all photons absorbed contribute to the QE. This is clearly a desirable feature as it implies that carrier collection from the QWs is very efficient allowing the increase in short circuit current. It is a good indicator that the QE of an QWSC could well approach that of a bulk cell with

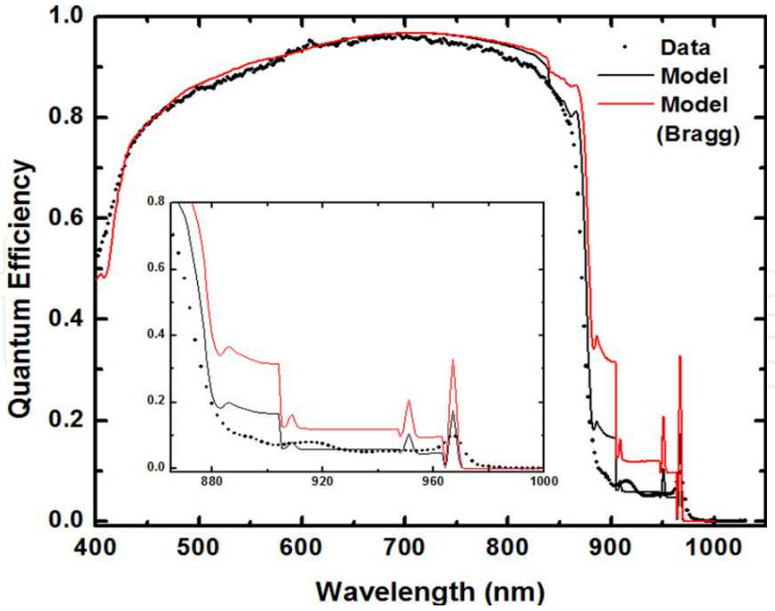

Figure 11. Modelled and experimental quantum efficiency versus wavelength for 5 well qt1897b sample from the Quantum photovoltaics Group of Imperial College. The inset shows the wavelength range dominated by the QW absorption with and without influence of DBR.

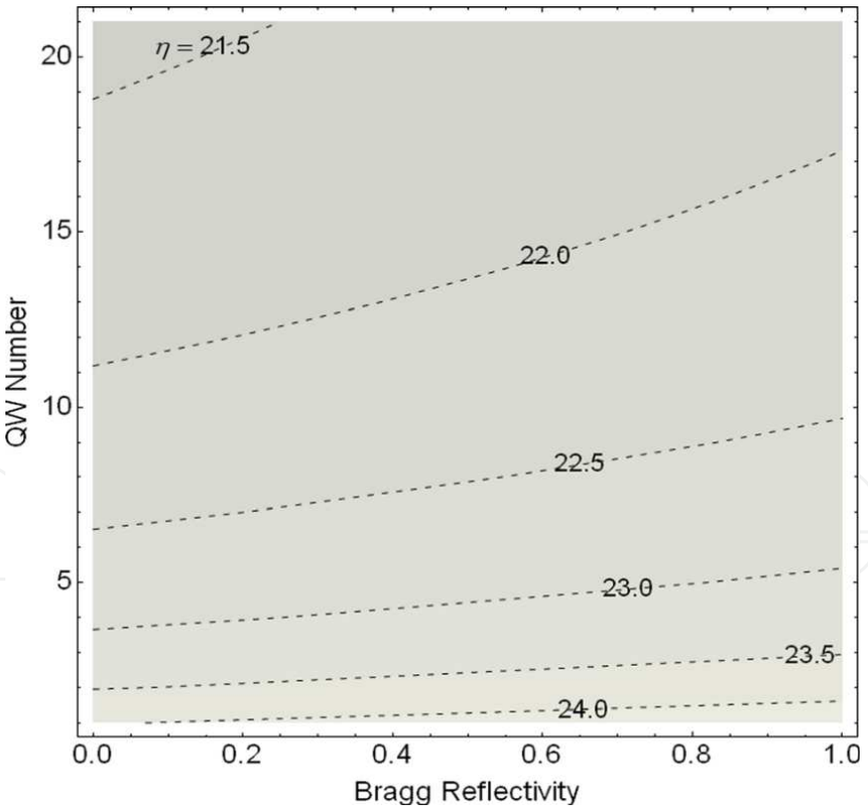

Figure 12. Contour plot for conversion efficiency as function of Bragg reflectivity and quantum well number. P composition y = 0.09, In composition x = 0.17 and L_W = 9.6 nm

http://dx.doi.org/10.5772/59616

a similar band-gap if the light could be confined inside the cell until it was completely absorbed.

For qt1897b solar cell, the dependence of conversion efficiency on back mirror reflectivity and quantum well number (N_W) is examined in Figure 12. This plot suggests that with the addition of a DBR in the device, fewer quantum wells are required to grow in the i-region in order to achieve high performance. In fact, low energy photons from the radiative recombination in the QWs can be reflected back into i-region and reabsorbed, lowering the radiative recombination current and improving the open-circuit voltage

It can be expected that SB-QWSC under concentration will be operating in a regime where recombination is dominated by radiative processes. Therefore, photon recycling effect is favoured under solar concentration when photons emitted from radiative recombination are subsequently reabsorbed by the solar cell. This can be explained as an increase in minority carrier lifetime or reduction in dark-current.This behavior is shown in Figure 13, where we have examined the conversion efficiency as a function of solar concentration for optimized $GaAs_{0.96}P_{0.04}/In_{0.03}Ga_{0.97}As/GaAs$ solar cell with 20 nm quantum well width. We used $r_A = 0.1$, $r_B = 0.95$ and resistive effects were neglected. It can be observed how the conversion efficiency should increase with solar concentration up to 1000 suns. In any concentration range, the DBR cell efficiency improvement over the non-DBR cell which is explained by the fact of the lower dark current in the DBR cell. This effect also causes that the net increase in conversion efficiency is lower with increasing N_W, as it can be noted in Figure 13.

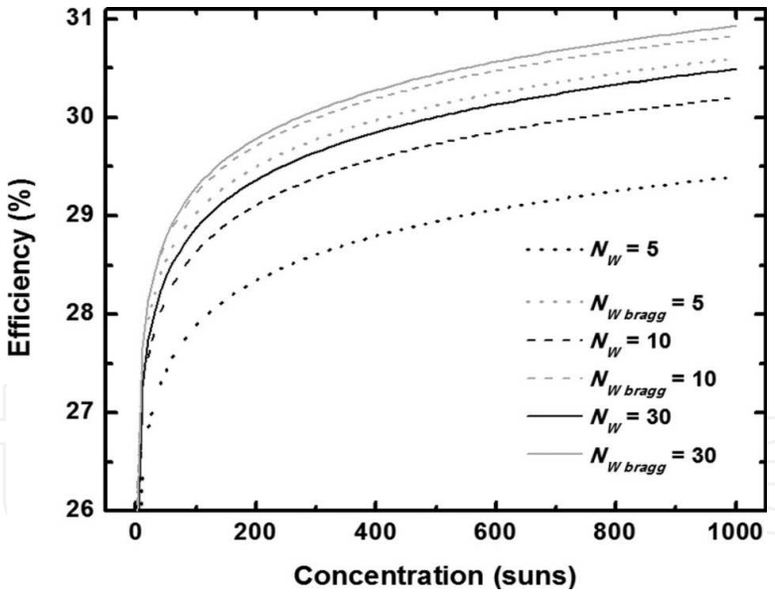

Figure 13. Conversion efficiency as a function of solar concentration for several $GaAs_{0.96}P_{0.04}/In_{0.03}Ga_{0.97}As/GaAs$ SB-QWSC which differ in the number of QW embedded within the i-region with and without influence of DBR.

3.3. GaAs/GaInNAs QWSC and SLSC

A recent alloy able to be used as well material in GaAs p-i-n solar cell is the GaInNAs. In order to investigate the $GaAs/Ga_{1-x}In_xN_yAs_{1-y}$ QWSC conversion efficiency, small nitrogen concentrations were considered to modify the quantum well depth. The lattice

matching condition to GaAs is met if the Indium and Nitrogen concentrations satisfy the relation $x = 2.85y$. The electron and hole concentrations, in GaAs base and emitter regions are $1.8 \times 10^{17} cm^{-3}$ and $2.3 \times 10^{18} cm^{-3}$, respectively, while their widths are $0.15 \mu m$ (p-region), $0.60 \mu m$ (i-region), and $0.46 \mu m$ (n-region). A 40 nm $Al_{0.8}Ga_{0.2}As$ window layer was incorporated into the p- region to reduce front surface recombination and a 70 nm MgF:SiN layer as ARC was used.

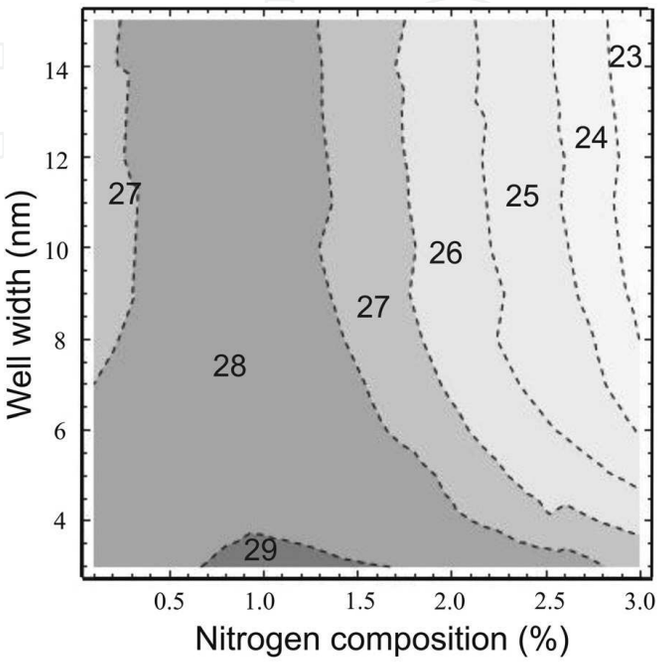

Figure 14. Contour plot of GaAs/GaInNAs QWSC efficiency as a function of the quantum well width and the nitrogen composition.

GaInNAs parameters were taken from reference [29]. High values of conversion efficiency are reached up to 3% N composition [30, 31], as depicted in Figure 14. The maximum values of efficiency are obtained for a narrow region around 1% of nitrogen composition and narrow quantum well widths. These N compositions correspond to shallow quantum wells, where the carrier generation overcomes the recombination. Also, for these N fractions a second quantum level appears in the heavy hole band slightly increasing photon absorption.

When the quantum wells are deeper (nitrogen percent increases) the carrier recombination increases and the conversion efficiency drops. In Figure 14 is shown the conversion efficiency as function of quantum well width. For 1% nitrogen composition, the conversion efficiency is almost insensitive to quantum well width due to a compensation effect, as there is a trade-off between quantum well width and quantum well number. Wider quantum wells absorbs more photons, but the amount quantum wells in the intrinsic region ($0.6 \mu m$) is smaller. On the other hand, narrow quantum wells have small photon absorption but it is possible to insert more of them in the intrinsic region. For other nitrogen compositions higher than 1%, the efficiency drops when the quantum well width increases because the carrier recombination is higher.

To study the case of GaAs/GaInNAs SLSC, keeping the other device parameters identical as it was defined for QWSC, the condition for resonant tunneling were calculated by the

http://dx.doi.org/10.5772/59616

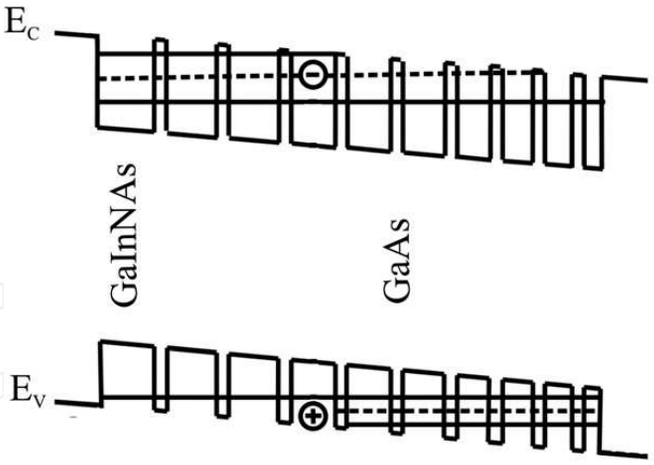

Figure 15. A variably spaced multiple quantum well (cluster) which enhances the resonant tunneling between adjacent wells.

well-known transfer matrix method without back-scattered wave. A variably spaced multiple quantum well or superlattice was considered. Figure 15 illustrates this particular superlattice unit that we have been refering as a cluster, in which the resonant tunneling character were obtained. The resonance takes place for an electric field of 12 kV/cm, which was obtained accounting uniform doping levels at the p- and n-regions, and intrinsic region width $0.60\mu m$. We have used a fixed field, which is a parameter in our model.

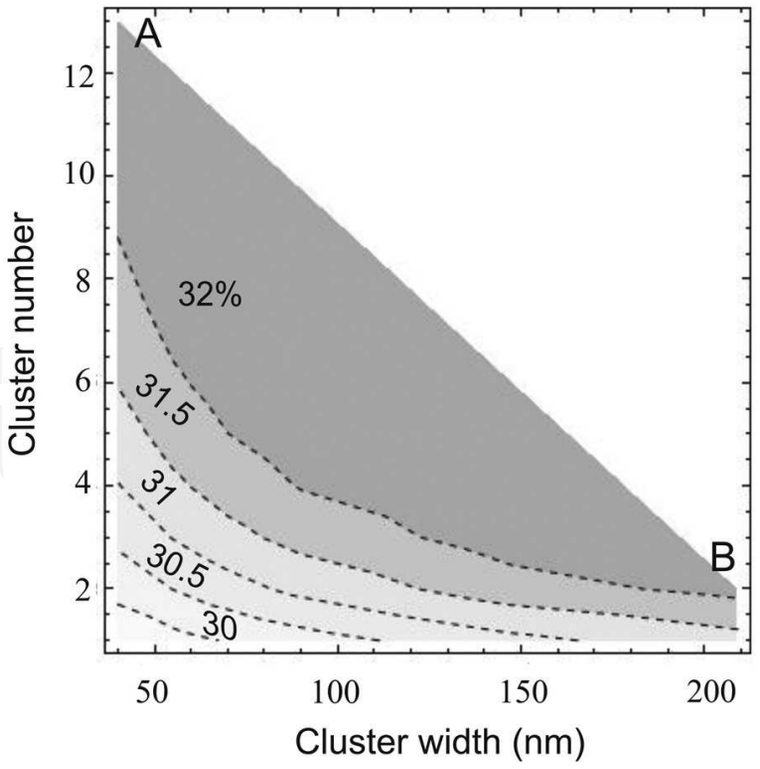

Figure 16. Contour plot of GaAs/GaInNAs SLSC efficiency as a function of the cluster width and number.

To study the GaAs/GaInNAs SLSC performance, it was considered a cluster composed of ten variably spaced multiple quantum wells optimized to maximise the resonant tunneling between adjacent wells. The GaInNAs quantum wells contains of 1% nitrogen composition and the GaAs barriers are 1 nm wide. A series of clusters are inserted in the intrisic region, independent from each other, in such a way that there is no coupling between neighboring clusters.

Figure 16 exhibits a contour plot of the conversion efficiency for the SLSC as a function of the cluster width and the number. If we compare these results with Figure 15 is evidenced that maximum SLSC conversion efficiencies are higher than those of QWSC by 3%. The AB contour in Figure 16 represents highest conversion efficiency obtained in the calculations. It can be also evidenced that the conversion efficiency rises as the width and the number cluster also increase, due to higher photon absorption.

4. Conclusions

A model for quantum well and superlattice solar cells was presented and applied to theoretically study qualitative trends in quantum well and superlattice solar cell performances. The findings from this study enhance our understanding of these devices and could provide a suitable guide for its designing. The model allows optimization the solar cell performance as a function of several of its parameters. The well and barrier band gaps, the width and depth of the wells, the amount of the wells in the intrinsic region are considered in the model to attain the best conversion efficiency.

We have shown theoretically that the insertion of multiple quantum wells into the intrinsic region of a p-i-n $Al_xGa_{1-x}As$ solar cell can enhance the conversion efficiency compared with its baseline cell. The quantum efficiency and the photocurrent for the AlGaAs/GaAs QWSC was calculated and compared with experimental results obtaining good agreement. These results, together with the agreement of the calculated open-circuit voltage with experimental values confirm the reliability of the model presented in this chapter.

GaAsP/InGaAs/GaAs strain-balanced solar cell was presented and studied. The effect of the electric field and the tensile and compressive stress, were carefully considered. The results of the modeling of SB-QWSC were also compared with experimental measurements successfully, validating again the suitability of the model. Following the model was used to determine the highest possible efficiencies for SB-QWSC containing quantum wells under varying degrees of strain. The strain-balanced multiple quantum well solar cells show a high conversion efficiency that makes it very attractive for their use in multijunction solar cells for space applications or concentrator photovoltaics based on a GaAsP/InGaAs/GaAs middle cell. Solar cells containing strain balanced QWs in a multijunction solar cell allow the absorption edge of each subcell to be independently adjusted.

We have shown a new type of photovoltaic device, the superlattice solar cell (SLSC), where coupled quantum wells or superlattices are inserted into the intrinsic region. The aim of this approach is the possibility of better tailor the photon absorption improving, at the same time, the transport of photogenerated carriers due to the tunneling along the nanostructure. The model adjusted to the superlattice solar cell case was then applied to GaAs/AlGaAs and GaAs/GaInNAs material systems. For the GaAs/AlGaAs case, was found photocurrent increase, and slight increments in the conversion efficiency over the QWSC. When applied the

model to GaAs/GaInNAs, was obtained the dependence of conversion efficiency as function of nitrogen composition and quantum well width, which allowed determining the range of these parameters where higher conversion efficiencies than in QWSC of the same material system are reached.

Besides, the GaAs/GaInNAs QWSC or SLSC show high conversion efficiency. That make them very attractive for space applications or for a triple-junction concentrator cell based on a GaAs/GaInNAs bottom cell that could reach 50% conversion efficiency. Because of the results that our model predicts haven't been compared nor confirmed experimentally, it would be interesting to see if future experiments will corroborate our findings.

Solar cell efficiency potential remains far greater than actual solar cell efficiencies, including those achieved in research laboratories. New approaches are necessary in order to increase the conversion efficiency and the quantum based solar cells could be a road to reach this goal.

5. Acknowledgments

Thanks to COZCYT for the partial financial support for this chapter.
J.C. Rimada acknowledges the International Centre for Theoretical Physics (ICTP) for partial funding under the TRIL programme.

Author details

Luis M. Hernández[1], Armando Contreras-Solorio[2], Agustín Enciso[2], Carlos I. Cabrera[2], Maykel Courel[3], James P. Connolly[4] and Julio C. Rimada[5*]

*Address all correspondence to: jcrimada@fisica.uh.cu; jcrimada@gmail.com

1 Faculty of Physics, University of Havana, Colina Universitaria, La Habana, Cuba

2 Academic Unit of Physics, Autonomous University of Zacatecas, Zacatecas, Mexico

3 Higher School in Physics and Mathematics, National Polytechnic Institute, Mexico, Mexico

4 Nanophotonics Technology Center, Polytechnic University of Valencia, Valencia, Spain

5 PV Laboratory, Institute of Materials Science and Technology (IMRE)- Faculty of Physics, University of Havana, La Habana, Cuba

References

[1] W Shockley, HJ Queisser (1961) Detailed balance limit of ef- ficiency of p-n junction solar cells. J. Appl. Phys; 32 510âĂŞ519. doi:10.1063/1.1736034

[2] K.W.J. Barnham, C. Duggan (1990) A new approach to high-efficiency multi-bandgap solar cells. J. Appl. Phys. 67 (7) 3490-3493

[3] M. Courel, J. C. Rimada, L. Hernández (2011) AlGaAs/GaAs superlattice solar cells. Progress in Photovoltaics: Res. Appl. 21 276-282 doi: 10.1002/pip.1178

[4] J. Nelson, M. Paxman, K. W. J. Barnham, J. S. Roberts and C. Button (1993) Steady-State Carrier Escape from Single Quantum Wells. IEEE Journal of Quantum Electronics, Vol. 29, No. 6 1460-1465. doi:10.1109/3.234396

[5] M. Paxman, J. Nelson, K. W. J. Barnham, B. Braun, J. P. Connolly, C. Button, J. S. Roberts and C. T. Foxon (1993) Modeling the Spectral Response of the Quantum Well Solar Cell. Journal of Applied Physics, Vol. 74, No. 1 614-621. doi:10.1063/1.355275

[6] T. Aihara, A. Fukuyama, Y. Yokoyama, M. Kojima, H. Suzuki, M. Sugiyama, Y. Nakano, and T. Ikari (2014) Detection of miniband formation in strain-balanced InGaAs/GaAsP quantum well solar cells by using a piezoelectric photothermal spectroscopy. Journal of Applied Physics, 116, 044509 doi: 10.1063/1.4887443

[7] Green, Martin A. and Emery, Keith and Hishikawa, Yoshihiro and Warta, Wilhelm and Dunlop, Ewan D. (2015) Solar cell efficiency tables (version 46). Progress in Photovoltaics: Research and Applications 23 (7) 805–812 doi: 10.1002/pip.2637

[8] P. R. Griffin, J. Barnes, K. W. J. Barnham, G. Haarpaint-ner, M. Mazzer, C. Zanotti-Fregonara, E. Grunbaum, C. Olson, C. Rohr, J. P. R. David, J. S. Roberts, R. Gray and M. A. Pate (1996) Effect of Strain Relaxation on Forward Bias Dark Currents in GaAs/InGaAs Multiquantum Well p-i-n Diodes. Journal of Applied Physics, Vol. 80, No. 10 5815-5820. doi:10.1063/1.363574

[9] N. J. Ekins-Daukes, K. W. J. Barnham, J. P. Connolly, J. S. Roberts, J. C. Clark, G. Hill and M. Mazzer (1999) Strain-Balanced GaAsP/InGaAs Quantum Well Solar Cells. Applied Physics Letters, Vol. 75, No. 26 495-497. doi:10.1063/1.125580

[10] D. C. Johnson, I. Ballard, K. W. J. Barnham, M. Mazzer, T. N. D. Tibbits, J. Roberts, G. Hill and C. Calder (2006) Optimisation of Photon Recycling Effects in Strain-Balanced Quantum Well Solar Cells. Proceedings of the 4th World Conference on Photovoltaic Energy Conversion, Hawaii, 7-12 May 2006 26-31

[11] M. Kondow, K. Uomi, A. Niwa, T. Kitatani, S. Watahiki and Y. Yazawa (1996) GaInNAs: A Novel Material for Long- Wavelength-Range Laser Diodes with Excellent High-Temperature Performance. Japanese Journal of Applied Physics, Vol. 35 1273-1275. doi:10.1143/JJAP.35.1273

[12] D. J. Friedman and S. R. Kurtz (2002) Breakeven Criteria for the GaInNAs Junction in GaInP/GaAs/GaInNAs/Ge Four-Junction Solar Cells. Progress in Photovoltaics, Vol. 10, No. 5 331-344. doi:10.1002/pip.430

[13] A. Freundlich, A. Fotkatzikis, L. Bhusal, L. Williams, A. Alemu, W. Zhu, J. A. H. Coaquira, A. Feltrin and G. Rad- hakrishnan (2007) III-V Dilute Nitride-Based Multi-Quantum Well Solar Cell. Journal of Crystal Growth, Vol. 301- 302, 993-996. doi:10.1016/j.jcrysgro.2006.11.256

[14] E. Reyes-Gómez, L. E. Oliveira and M. de Dios-Leyva (2005) Quasi-Bond States and Intra-Band Transition Energies in GaAs-(Ga,Al)As Variably Spaced Semiconductor Super- lattices. Physica B, Vol. 358, No 1-4, 269-278. doi:10.1016/j.physb.2005.01.462

[15] J. C. Rimada, L. Hernández, J. P. Connolly and K. W. J. Barnham (2007) Conversion Efficiency Enhancement of AlGaAs Quantum Well Solar Cells. Microelectronics Journal, Vol. 38, No. 4-5 513-518. doi:10.1016/j.mejo.2007.03.007

[16] J.C. Rimada, L. Hernández (2001) Modeling of ideal AlGaAs quantum well solar cells. Microelectronics Journal. Vol. 32, 719-723

[17] N.G. Anderson (1995) Ideal theory of quantum well solar cells. J. Appl.Phys. 78 (3) 1850 - 1861

[18] G. Bastard (1988) Wave Mechanics Applied to Semiconductor Heterostructures. Editions de Physique, Paris

[19] H. Mathieu, P. Lefebre, P. Christol (1992) Simple analytical method for calculating exciton binding energies in semiconductor quantum wells. Phys. Rev. B 46 (1) 4092-4101

[20] Petroff, P. M. and Logan, R. A. and Savage, A. (1980) Nonradiative Recombination at Dislocations in III-V Compound Semiconductors. Phys. Rev. Lett., 44(4),287–291, doi: 10.1103/PhysRevLett.44.287

[21] B. Browne, A. Ioannides, J. Connolly, K. Barnham, J. Roberts, R. Airey, G. Hill, G. Smekens and J. Van Begin (2008) Tandem quantum well solar cells. Proceedings of 33rd IEEE Photovoltaic Specialists Conference, San Diego, CA. USA.

[22] N. J. Ekins-Daukes, K. Kawaguchi, and J. Zhang (2002) Strain-Balanced Criteria for Multiple Quantum Well Structures and Its Signature in X-ray Rocking Curves. Crystal Growth and Design 2 (4) 287–292

[23] Adams, J. G. J. and Browne, B. C. and Ballard, I. M. and Connolly, J. P. and Chan, N. L. A. and Ioannides, A. and Elder, W. and Stavrinou, P. N. and Barnham, K. W. J. and Ekins-Daukes, N. J (2011) Recent results for single junction and tandem quantum well solar cells. Progress in Photovoltaics: Research and Applications 19 (7) 865-877 doi:10.1002/pip.1069

[24] P. Harrison (2005) Quantum Wells, Wires, and Dots. John Wiley & Sons, Ltd., 219-230

[25] Varonides AC (2004) Tunneling photoconductivity computations of multi-quantum well p-i(nano)-n photovoltaic nanostructures by means of the causal Green's function. Thin Solid Films 451-452: 393-396

[26] J. C. Rimada , L. Hernández, J. P. Connolly and K. W. J. Barnham (2005) Quantum and conversion efficiency calculation of AlGaAs/GaAs multiple quantum well solar cells. Physica Status Solidi 242, 1842

[27] CI Cabrera, JC Rimada, JP Connolly, L Hernández (2013) Modelling of GaAsP/InGaAs/GaAs strain-balanced multiple-quantum well solar cells. Journal of Applied Physics 113, 024512

[28] C. I. Cabrera, J. C. Rimada, L. Hernández, J. P. Connolly, A. Enciso, and D. A. Contreras-Solorio (2014) Anisotropic emission and photon-recycling in strain-balanced quantum well solar cells. Journal of Applied Physics 115, 164502

[29] Sheng-Horng Yen, Mei-Ling Chen, Yen-Kuang Kuo (2007) Gain and threshold properties of InGaAsN/GaAsN material system for 1.3μm semiconductor lasers. Optics & Laser Technology, Volume 39, Issue 7 1432-1436 doi:10.1016/j.optlastec.2006.10.003.

[30] M.Courel, J.C.Rimada, L.Hernández (2012) GaAs/GaInNAs quantum well and superlattice solar cells. Appl. Phys. Lett. 100, 073508.

[31] M.Courel, J.C.Rimada, L.Hernández (2012) An approach to high efficiencies using GaAs/GaInNAs multiple quantum well and superlattice solar cell. J. Appl. Phys. 112, 054511.